

Monte Carlo simulation of GaN/InN mixtures

John A. Purton,*^a Mikhail Yu. Lavrentiev^{†b} and Neil L. Allan^b

Received 28th June 2004, Accepted 1st November 2004

First published as an Advance Article on the web 2nd December 2004

DOI: 10.1039/b409770j

Exchange Monte Carlo calculations in the semi-grand canonical ensemble are used to determine the mixing properties of GaN and InN in *both* the wurtzite and zinc blende structures. Inter-atomic potentials are obtained *via* empirical fitting to the experimental, bulk properties of the end member materials. The difference in structure is reflected in the variation of the enthalpy of mixing with composition and phase diagrams for the hexagonal and cubic phases. The calculated consolute temperature is ≈ 1725 K, in line with previous calculations. The calculated phase diagrams for the two structures are markedly asymmetric with the maximum in the binodals lying markedly on the Ga rich side. Our results are compared with available experimental data.

Introduction

The last decade has seen remarkable progress in the development of optical and electronic devices such as light-emitting diodes and laser diodes, based on the group-III nitrides AlN, GaN, InN and their alloys. Important examples are active optoelectronic devices operating in the green, blue and ultraviolet spectral region.¹ The band gaps of InN, GaN and AlN are 1.89, 3.44 and 6.28 eV respectively.² Alloys of these end members have been fabricated in order to “engineer the band gap” and thus manufacture materials for novel devices.

Understanding the thermodynamic properties and atomic structure of $\text{In}_x\text{Ga}_{1-x}\text{N}$ alloys is crucial to the systematic fabrication of these devices. Under ambient conditions GaN, InN and their alloys have been observed to crystallise in the hexagonal wurtzite structure (*h*- $\text{Ga}_x\text{In}_{1-x}\text{N}$).³ The wurtzite structure has also been found for films grown using molecular beam epitaxy (MBE),⁴ metal-organic chemical vapour phase deposition (MOCVD),⁵ and hybrid vapor phase epitaxy.⁶ More recently thin films of these nitrides and their alloys have been grown with the cubic zinc blende structure (*c*- $\text{In}_x\text{Ga}_{1-x}\text{N}$).^{7,8} A common feature of the nitride alloy epitaxies is the strain due to the lattice mismatch and different thermal expansion coefficients. The lattice mismatch between InN and GaN is 10.7% and 15% for the hexagonal *a* and *c* lattice parameters respectively and $\approx 10\%$ for the cubic lattice parameter of the zinc blende structure. The large difference in the equilibrium lattice constants and bond lengths results in internal strain and phase separation. In addition, there are two significant structural differences between the bond distances in the wurtzite and zinc blende modifications:⁹ (i) every ion in the zinc blende structure (Fig. 1a) has four nearest neighbours all with the same bond length. In the wurtzite form (Fig. 1b) there is also four nearest neighbours, but one bond length is greater than the remaining three; (ii) in the zinc blende structure there is only one second neighbour cation-anion bond distance compared with three in the wurtzite structure.

Since the pioneering work of Osamura *et al.*,^{3,10} based on infrared reflectivity of polycrystalline films, evidence for phase separation in *h*- and *c*- $\text{In}_x\text{Ga}_{1-x}\text{N}$ has been investigated using X-ray diffraction (XRD), transmission electron microscopy (TEM), Raman scattering, scanning tunneling microscopy and luminescence spectroscopy. A number of authors have studied $\text{In}_x\text{Ga}_{1-x}\text{N}$ films grown using either MBE or MOCVD, examining the structures using XRD and TEM, and have reported the formation of a solid solution of approximately

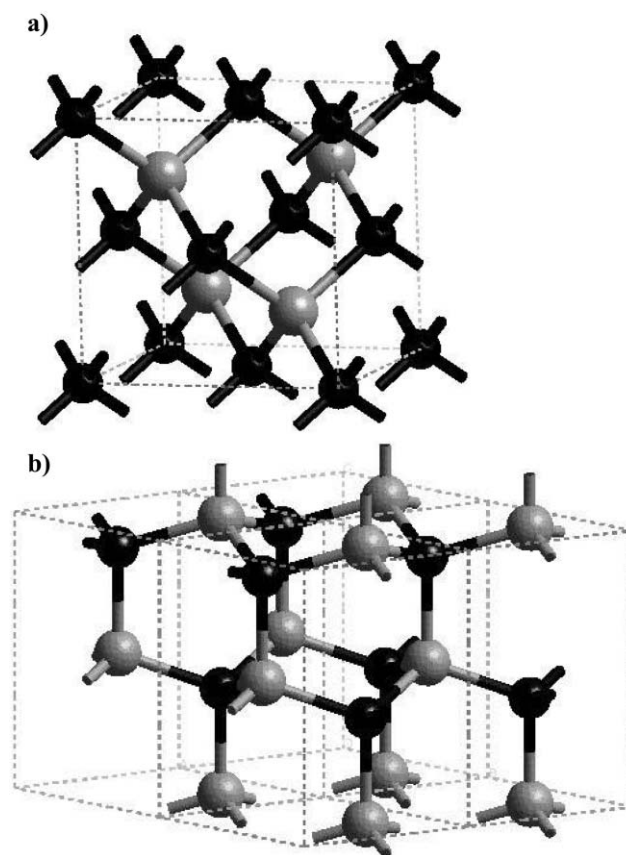


Fig. 1 (a) Zinc blende structure; (b) wurtzite structure. Lighter spheres are cations, darker anions.

[†] On leave from Institute of Inorganic Chemistry, 630090 Novosibirsk, Russia.

*j.a.purton@dl.ac.uk

30% In in GaN.^{4,5} Singh and co-workers¹¹ grew thick films using MBE and determined their structures using XRD. In agreement with previous results^{4,5} they concluded that at 973–1073 K the maximum In content is $x < 0.3$. They also describe¹¹ techniques to obtain alloys with up to 80% In without any detectable phase separation. In contrast, indirect experimental evidence for compositional fluctuations in $\text{In}_x\text{Ga}_{1-x}\text{N}$ alloys with lower In contents ($x \leq 0.1$) has also been reported.¹² More recently Raman scattering has been employed to study both *h*- and *c*- $\text{In}_x\text{Ga}_{1-x}\text{N}$ for compositions $x = 0.1$ ¹³ and $x = 0.07, 0.19$ and 0.33 .⁸ Indium rich inclusions were identified in all samples.

Because of the potential applications of $\text{In}_x\text{Ga}_{1-x}\text{N}$ alloys there have been a number of theoretical studies of the mixing properties of GaN and InN and these have included both valence force-field and electronic structure calculations. Ho and Stringfellow¹⁴ and Saito and Arakawa¹⁵ used a valence force-field method coupled with the regular solution model to derive the phase diagram of *h*- $\text{In}_x\text{Ga}_{1-x}\text{N}$ alloys. Reference 16 employed density functional theory (DFT) calculations to determine the mixing enthalpy, but considered only one configuration and assumed the regular solution model, whilst Teles *et al.* used pseudopotential calculations¹⁷ and the generalised quasichemical approach to determine the phase stability of the cubic alloy. The computational results agree qualitatively yet significant differences are apparent. For example, the calculated consolute temperatures determined are 1250, 1417, ≈ 1950 and 1295 K in refs. 14, 15, 16 and 17 respectively. The phase diagrams of Ho and Stringfellow¹⁴ and van Schilfgaarde *et al.*¹⁶ are symmetric, while, in contrast, the phase diagrams of Saito and Arakawa¹⁵ and Teles *et al.*¹⁷ are asymmetric with greater miscibility of Ga in InN than In in GaN. Moreover, these studies have not determined the effect of the different crystal structures on the mixing properties of the GaN and InN. Thus in this paper analytical potentials are derived for the Ga–In–N system by fitting to experimental properties of the end member compounds. These empirical potentials are used to calculate directly the phase diagram from atomistic Monte Carlo simulations that allow us to consider the full structural relaxation around dopant ions, numerous ionic configurations and thermal/vibrational effects on the crystal structure and phase diagram. In addition, we interpret and compare the mixing properties of $\text{In}_x\text{Ga}_{1-x}\text{N}$ in both wurtzite and zinc blende forms.

Methodology

The basis for our calculations is the well-known Monte Carlo (MC) method modified as described below. In simulations of ionic non-stoichiometric materials using “standard” MC, kinetic barriers prevent sampling the whole of the configurational space since almost always only one cation arrangement is sampled (the initial configuration), which is chosen at random. We only describe briefly the Monte Carlo Exchange (MCX) technique, since it has been discussed in detail in our previous papers.^{18,19} In order to calculate the phase diagram *both* the atomic configuration *and* the atomic coordinates of all the atoms in the system are modified. In any one MC cycle one of four alterations to the system are made at random:

(i) an atom is displaced by a random amount. The maximum changes in the atomic displacements are governed by a variable r_{max} . The magnitude of this parameter is adjusted automatically during the simulation to maintain an acceptance/rejection ratio of approximately 0.5.

(ii) a change in cell volume. The parameter v_{max} controls the maximum allowed change in volume and is controlled in a similar manner to r_{max} .

(iii) attempted exchange of In and Ga ions using an exchange bias technique.¹⁹

(iv) a semi-grand canonical substitution.^{19,20} In this method we evaluate the potential energy change $\Delta U_{\text{B/A}}$ which would result if one species, B, were to be converted into another, A. This change in energy is related to the corresponding change in chemical potential $\Delta\mu_{\text{B/A}}$ by

$$\Delta\mu_{\text{B/A}} = -k_{\text{B}}T \ln \left\langle \frac{N_{\text{B}}}{N_{\text{A}} + 1} \exp(-\Delta U_{\text{B/A}}/k_{\text{B}}T) \right\rangle \quad (1)$$

Thus for GaN–InN, we evaluate the energy associated with the conversion of a randomly chosen Ga ion to an In ion, $\Delta U_{\text{Ga/In}}$ and the reverse transformation. We emphasize that the change of Ga into In, and *vice versa*, is only a temporary substitution to determine the difference in chemical potential. After eqn. (1) is evaluated, the identity of the randomly chosen ion reverts to Ga (In) and the simulation continued as before. The semi-grand canonical ensemble is used in preference to the grand canonical ensemble since good statistics for $\Delta\mu_{\text{B/A}}$ can readily be achieved. The calculated values of $\Delta U_{\text{Ga/In}}$ are used to determine the excess free energy of mixing as described below. The Metropolis algorithm²¹ is used to accept or reject any move, volume change or ion exchange. The Monte Carlo calculations were based upon simulation cells consisting of 256 ions ($4 \times 4 \times 4$ unit cells) and 216 ions ($3 \times 3 \times 3$ unit cells) for the wurtzite and zinc blende structures respectively. The number of iterations for each simulation consisted of 2×10^6 and 5×10^7 cycles for the equilibration and production stages respectively.

A number of potential models exist for the simulation of GaN and InN and have been based either on an ionic^{22,23} or a covalent model.^{24,25} The former consists of a long-range Coulombic term and a short-range potential V_{ij} of Buckingham form:

$$V_{ij} = A \exp(-r_{ij}/\rho) - Cr_{ij}^{-6} \quad (2)$$

where r_{ij} is the interionic separation between ions labelled *i* and *j*, and *A*, ρ and *C* are parameters obtained as described below. Polarisation of the nitrogen atoms is treated by modelling the electrons with a massless shell harmonically coupled to the core. Zapol *et al.*²² and Chisholm *et al.*²³ have argued that an ionic model, using partial charges obtained by Mulliken population analysis and first principles calculations, is appropriate for GaN and InN. Such a model was then employed successfully to determine the elastic and vibrational properties of these nitrides.^{22,23} Alternatively, covalent models (involving no assignment of partial charges) have also been developed as for other semiconducting materials.^{24,25} For example, the Stillinger–Weber potential²⁶ has been employed to study stacking faults in Al, Ga, and In nitrides.²⁴

Table 1 Interatomic pair potential parameters for the $\text{Ga}_x\text{In}_{1-x}\text{N}$ system

Atom types	A/eV	$\rho/\text{\AA}$	$C/\text{eV \AA}^6$
N–N	21751.84	0.2688	20.0
Ga–N	859.56	0.3080	0.00
In–N	679.71	0.3582	0.00

^a The parameters are for the Buckingham pair potential $V_{ij} = A\exp(-r_{ij}/\rho) - Cr_{ij}^{-6}$ (see text).

We have adopted an approach similar to that of Zapol *et al.*²² and Chisholm *et al.*²³ and have used partial charges, in which the Ga, In atoms are assigned a charge of $+2e$, and the N atom a charge of $-2e$. However, these potential sets^{22,23}

used the shell model and have a large value for the C parameter (eqn. (2)), which make them unsuitable for MC calculations, where a large range of internuclear separations are sampled explicitly during the course of the simulations. In the present work, we have used a rigid ion model, in which the interatomic potentials for the end-member compounds were obtained by fitting to the structure and elastic properties. The resulting interatomic potentials for InN and GaN are presented in Table 1 and in Table 2 we compare results obtained with our new potential with experiment^{27–29} and with values calculated in references 22, 23 and 30. The values of our final calculated properties are in excellent agreement with experiment. We note also from Table 2 that the calculated lattice enthalpy is lower for the wurtzite phase of both

Table 2 Calculated and experimental properties of wurtzite and zinc blende GaN and InN

Property	GaN (this work)	GaN (experiment/ <i>ab initio</i>)	GaN ²²	GaN ²³
<i>Wurtzite</i>				
Lattice parameters/ \AA				
a	3.222	3.19 ^a	3.227	3.20
c	5.154	5.19 ^a	5.158	5.14
Ga–N distance/ \AA	1.951	1.949 ^a	1.955	1.941
	1.988	1.957	1.986	1.979
Lattice enthalpy/ eV ion^{-1}	–20.76		–21.16	–21.31
Elastic constants/GPa				
C_{11}	378.5	374.2 ^b	386.3	410.4
C_{12}	136.8	141.2 ^b	159.8	161.4
C_{13}	120.2	98.1 ^b	141.3	141.7
C_{33}	378.2	388.6 ^b	391.2	413.0
C_{44}	120.2	98.3 ^b	113.2	124.5
<i>Zinc blende</i>				
Lattice parameters/ \AA				
A	4.523	4.46 ^c	4.53	4.504
Ga–N distance/ \AA	1.959	1.944	1.962	1.950
Lattice enthalpy/ eV ion^{-1}	–20.71		–21.12	–21.26
Elastic constants/GPa				
C_{11}	288.7	296.0 ^c	299.6	315.3
C_{12}	169.5	154.0 ^c	190.7	195.2
C_{44}	167.1	206.0 ^c	159.5	169.5
Property	InN (this work)	InN (experiment)	InN ²³	
<i>Wurtzite</i>				
Lattice Parameters/ \AA				
a	3.558	3.533 ^d	3.53	
c	5.633	5.693 ^d	5.69	
In–N distance/ \AA	2.151	2.135	2.135	
	2.179	2.161	2.198	
Lattice enthalpy/ eV ion^{-1}	–18.48		–19.41	
Elastic constants/GPa				
C_{11}	206.2	223.0 ^b	297.5	
C_{12}	83.3	115.0 ^b	107.4	
C_{13}	72.7	92.0 ^b	108.7	
C_{33}	201.9	224.0 ^b	250.5	
C_{44}	65.4	48.0 ^b	89.4	
<i>Zinc blende</i>				
Lattice parameters/ \AA				
a	4.981	4.92 ^c	4.965	
In–N distance/ \AA	2.157	2.136	2.150	
Lattice enthalpy/ eV ion^{-1}	–18.44		–19.37	
Elastic constants/GPa				
C_{11}	153.8	184 ^c	233.4	
C_{12}	98.5	116 ^c	133.2	
C_{44}	100.9	177 ^c	103.1	

^a Xia *et al.*²⁷ ^b Reeber *et al.*²⁸ ^c Kim *et al.*³⁰ ^d Edger.²⁹ ^e Our results are compared to experiment^{27–29}, previous atomistic calculations using shell model potentials (references 22 and 23) and *ab initio* calculations.³⁰

end-members, showing it to be the most stable phase for both nitrides in the static limit.

Results and discussion

The Monte Carlo calculations were performed on GaN–InN solid solutions adopting both the wurtzite and the zinc blende structure at temperatures between 800 K and 1800 K. During the production part of the calculations we monitored the enthalpy of the system and the chemical potential difference between Ga and In ions.

We consider first the enthalpies of mixing, ΔH_{mix} , and their variation with composition. Fig. 2a and b display the calculated values of ΔH_{mix} for the *h*- and *c*- $\text{In}_x\text{Ga}_{1-x}\text{N}$ solid solutions over a range of temperatures. The curves have a maximum at $x \approx 0.50$. But they are not symmetric about the maximum with higher values of ΔH_{mix} on the Ga rich side, *i.e.* the GaN end member is less tolerant of In than the InN lattice of Ga. It is important to stress that the method applies no constraints on the form and symmetry of the ΔH_{mix} vs.

composition curve. The calculated values of ΔH_{mix} at 800 K for *h*- and *c*- $\text{In}_x\text{Ga}_{1-x}\text{N}$ at the maximum are ≈ 0.076 and 0.084 eV per cation–anion pair respectively, *i.e.* the magnitude of the enthalpy of mixing at 800 K for the zinc blende structure is $\approx 9\%$ greater than that for the wurtzite. This reflects the difference in structure. ΔH_{mix} for the wurtzite phase is the more sensitive to temperature so that at 1800 K the opposite is true (ΔH_{mix} values are 0.097 and 0.090 for *h*- and *c*- $\text{In}_x\text{Ga}_{1-x}\text{N}$ respectively). Nevertheless ΔH_{mix} varies less as a function of temperature than the Pd–Rh system, where similar calculations indicate ΔH_{mix} almost doubles over a similar temperature range.³¹ Our calculated values of ΔH_{mix} are slightly greater than the value of ≈ 0.055 eV per cation–anion pair in reference 17 but less than the value of 0.13 eV per cation–anion pair reported in references 14 and 15.

The calculation of the phase diagram requires the determination of *free energy differences* rather than absolute values, which can be achieved using the semi-grand canonical ensemble described above. We show the calculated values of $\Delta\mu_{\text{Ga/In}}$ in Fig. 3a and b for both the wurtzite and zinc blende

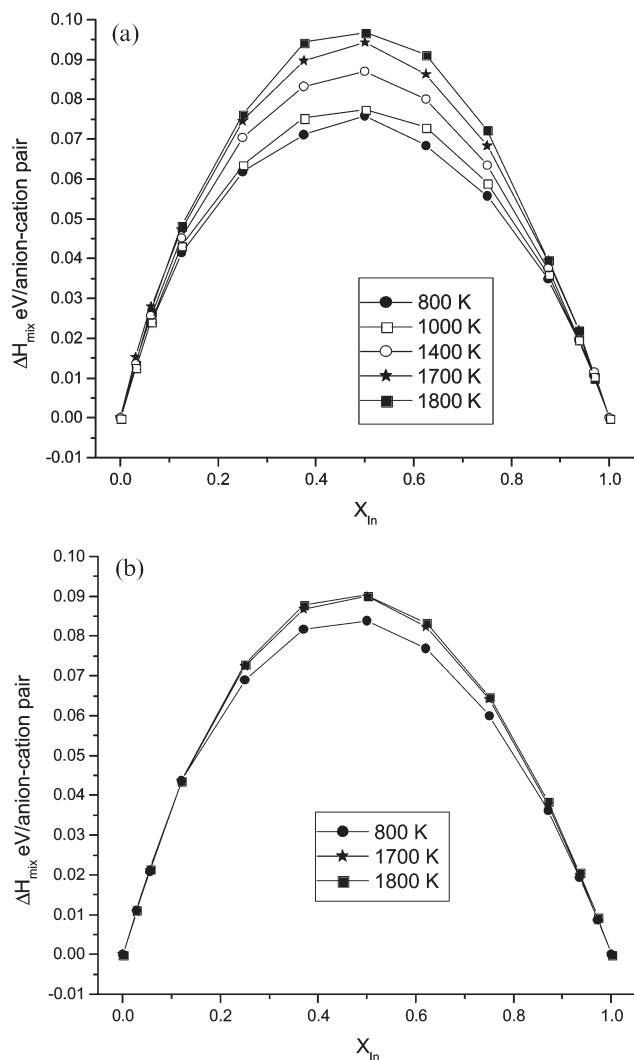


Fig. 2 Calculated values of the enthalpy of mixing, ΔH_{mix} , in eV per cation–anion pair for *h*- $\text{In}_x\text{Ga}_{1-x}\text{N}$ (a) and *c*- $\text{In}_x\text{Ga}_{1-x}\text{N}$ (b).

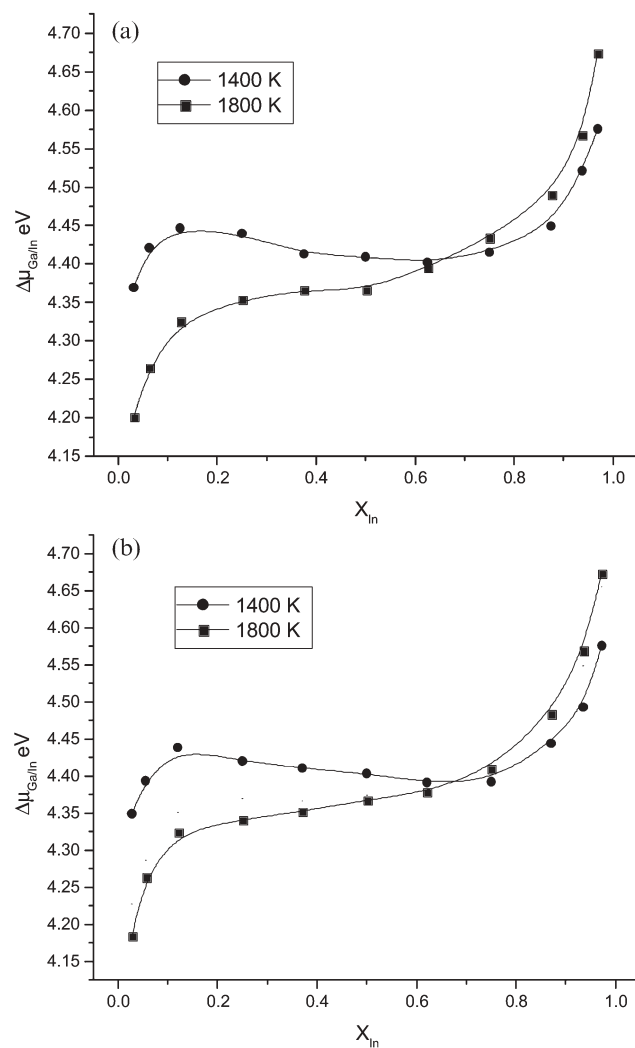


Fig. 3 Calculated variation of $\Delta\mu_{\text{Ga/In}}$ ($= \mu_{\text{In}} - \mu_{\text{Ga}}$) as a function of $\text{In}_x\text{Ga}_{1-x}\text{N}$ alloy composition for a) wurtzite and b) zinc blende structures.

structures respectively. The existence of a minimum and maximum in a $\Delta\mu_{(x)}$ curve indicates a miscibility gap at that temperature. For both phases it is clear from the shape of these curves that 1400 K corresponds to a temperature below the consolute temperature, and the formation of one- and two-phase regions at different compositions. For both structures the $\Delta\mu_{(x)}$ curve for 1700 K is just below the calculated consolute temperature, as indicated by the shape of the curves (not shown in Fig. 3) in which the stationary points evident at 1400 K have almost disappeared. At 1800 K the stationary points are not present, as is clear from Fig. 3, and this temperature is above the consolute temperature.

To calculate the phase diagram, the calculated values of $\Delta\mu_{(x)}$ are fitted¹⁹ to eqn. (3), as shown by the full lines in Fig. 3:

$$\frac{\Delta\mu}{k_B T} = \ln\left(\frac{x}{1-x}\right) + ax + bx^2 + cx^3 \quad (3)$$

By integrating eqn. (3) with respect to composition we obtain the variation in free energy with x at each temperature. In Fig. 4a and b we plot calculated values of ΔG_{mix} vs. x at 1400 and 1800 K for h - and c - $\text{In}_x\text{Ga}_{1-x}\text{N}$ respectively. Fig. 4

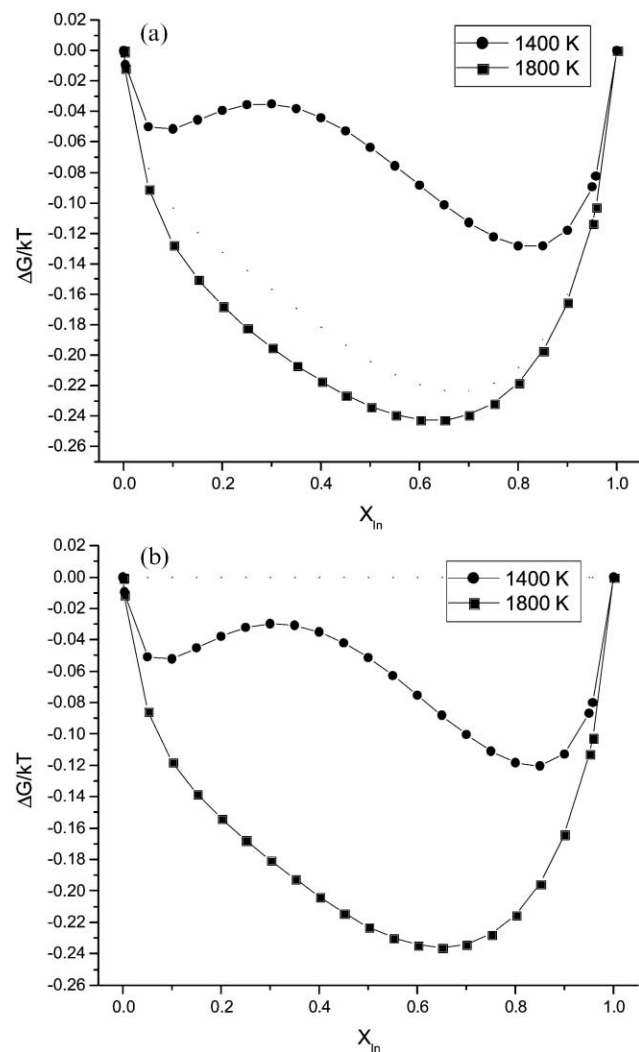


Fig. 4 Calculated variation of ΔG_{mix} for $\text{In}_x\text{Ga}_{1-x}\text{N}$ with alloy composition for a) wurtzite and b) zinc blende structures.

confirms that for h - and c - $\text{In}_x\text{Ga}_{1-x}\text{N}$ at 1400 K, one- and two-phase regions are formed at different compositions, and hence that this temperature lies below the consolute temperature. At 1800 K, the dependence of $\Delta G_{\text{mix}}(x)$ at all compositions is consistent with complete miscibility for both h - and c - $\text{In}_x\text{Ga}_{1-x}\text{N}$. Given curves as in Fig. 4, a straightforward common tangent construction at each temperature yields the phase diagrams in Fig. 5a and b. Thus, by performing calculations at several temperatures, the consolute temperatures were determined to be 1725 ± 13 K for both phases. The consolute temperature calculated using alternative methodologies ranges from 1295 to 1950 K.¹⁴⁻¹⁷ As in the calculations reported in ref. 17 we find that the binodal curves are asymmetric, and slanted towards the Ga end member such that the apex is at $x \approx 0.25$, *i.e.* the Ga ion is more soluble in InN than In in GaN. Although the consolute temperatures of both phases are very similar, there are important differences between the phase diagrams. The phase diagram for h - $\text{In}_x\text{Ga}_{1-x}\text{N}$ is somewhat more asymmetric than that for the cubic form and at temperatures ≥ 1400 K Ga is more soluble in h - $\text{In}_x\text{Ga}_{1-x}\text{N}$ than in c - $\text{In}_x\text{Ga}_{1-x}\text{N}$. The spinodal

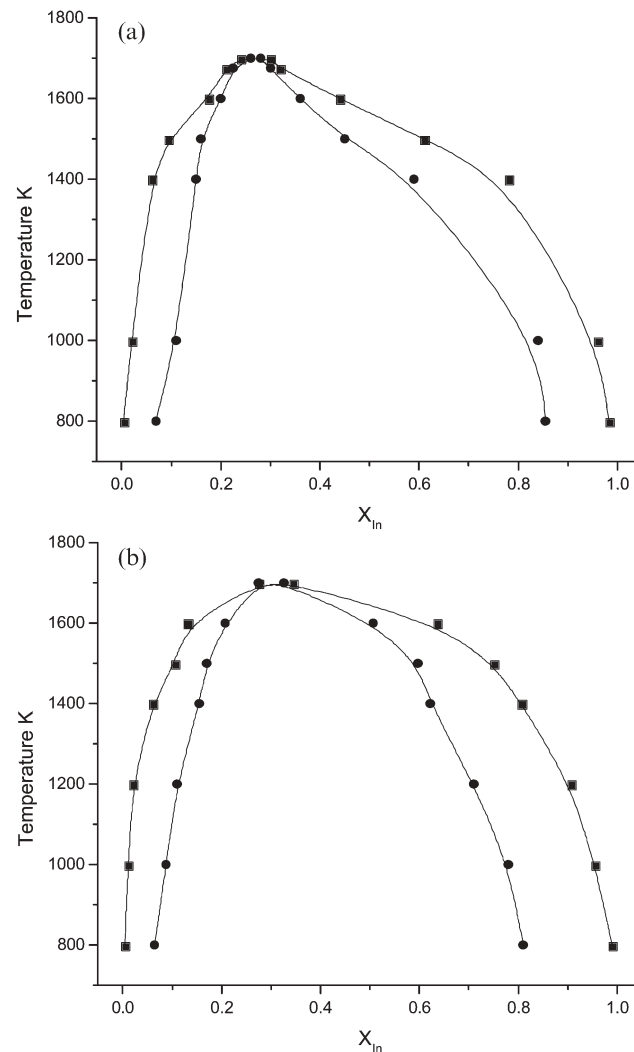


Fig. 5 Calculated phase diagram for a) h - and b) c - $\text{Ga}_x\text{In}_{1-x}\text{N}$. Solid squares mark the binodal, solid circles the spinodal.

curves, also plotted in the phase diagrams in Fig. 5a and b, define the region where a single phase is kinetically as well as thermodynamically unstable with respect to the formation of two separate phases.

Detailed comparison with experiment is difficult since the phase diagram of these alloys has not been determined precisely and our calculations probe the thermodynamic stability of the mixtures and do *not* take into account kinetic barriers. Despite this we can nevertheless draw a number of conclusions. At a typical growth temperature for a thin film of 1000 K we predict the solubility limit of InN in GaN to be approximately 5%. Our calculations thus agree with recent Raman scattering experiments that identified In rich inclusions in both *h*- and *c*-In_xGa_{1-x}N ($x = 0.1^{13}$ and $x = 0.07, 0.19$ and 0.33^8). However, we predict that the solubility is increasing rapidly in this region and the phase diagrams also indicate a wide range between binodal and spinodal curves so that an alloy may exist as a metastable phase.

Conclusions

We have derived a set of interatomic potentials for the system Ga–In–N using both *ab initio* and empirical methods. These potentials have been demonstrated to reproduce accurately the properties of the end member compounds. The MC calculations, based on interatomic potentials, take into account local relaxations and the vibrational effects of the ions and can be applied to different crystal structures of the same compound. With this in mind, we have determined the mixing properties of GaN and InN in *both* the wurtzite and zinc blende structures. The enthalpy of mixing for the zinc blende phase is less sensitive to temperature than for wurtzite. The difference in the enthalpies of mixing is reflected in the structure of the phase diagrams. The calculated consolute temperature is approximately 1725 K for both the cubic and the hexagonal solid solutions. Our results are in agreement with experimental observations^{8,13} concerning the phase stability of these alloys. We hope our paper prompts further experimental studies of this interesting system.

John A. Purton,^{*a} Mikhail Yu. Lavrentiev^{†b} and Neil L. Allan^b

^aCCLRC, Daresbury Laboratory, Warrington, UK, WA4 4AD.

E-mail: j.a.purton@dl.ac.uk; Fax: 44 1925 60388; Tel: 44 1925 603785

^bSchool of Chemistry, University of Bristol, Cantock's Close, Bristol, UK, BS8 1TS. Fax: 44 117 925 1295; Tel: 44 117 928 8308

References

- 1 S. Nakamura and G. Fasol, *The Blue Laser Diode*, Springer, Berlin, 1997.

- 2 Y. Wu, B. P. Keller, S. Keller, D. Kapolnek, P. Kosodoy, S. P. Denbaars and J. K. Mishra, *Appl. Phys. Lett.*, 1996, **69**, 1438.
- 3 K. Osamura, S. Naka and Y. Murakami, *Solid State Commun.*, 1972, **11**, 617.
- 4 D. Doppalapudi, S. N. Basu, K. F. Ludwig and T. D. Moustakas, *J. Appl. Phys.*, 1998, **84**, 1389.
- 5 N. A. El-Masry, E. L. Piner, S. X. Liu and S. M. Bedair, *Appl. Phys. Lett.*, 1998, **72**, 40.
- 6 Y. Sato and S. Sato, *Jpn. J. Appl. Phys.*, 1997, **36**, 4295.
- 7 A. Tabata, J. R. Leite, A. P. Lima, E. Silveira, V. Lemos, T. Frey, D. J. As, D. Shikora and K. Lischka, *Appl. Phys. Lett.*, 1998, **72**, 1095.
- 8 E. Silveira, A. Tabata, J. R. Leite, R. Trentin, T. Frey, D. J. As, D. Shikora and K. Lischka, *Appl. Phys. Lett.*, 1999, **75**, 3602.
- 9 T. Mattila and A. Zunger, *J. Appl. Phys.*, 1999, **85**, 160.
- 10 K. Osamura, S. Naka and Y. Murakami, *J. Appl. Phys.*, 1975, **46**, 3432.
- 11 R. Singh, D. Doppalapudi, T. D. Moustakas and L. T. Romano, *Appl. Phys. Lett.*, 1997, **70**, 1089.
- 12 S. Chichibu, T. Azuhata, T. Sota and S. Nakamura, *Appl. Phys. Lett.*, 1997, **70**, 2822.
- 13 D. Behr, J. Wagner, A. Ramakrishnan, H. Obloh and K.-H. Bachem, *Appl. Phys. Lett.*, 1998, **73**, 241.
- 14 I.-H. Ho and G. B. Stringfellow, *Appl. Phys. Lett.*, 1996, **69**, 2701.
- 15 T. Saito and Y. Arakawa, *Phys. Rev. B*, 1999, **60**, 1701.
- 16 M. van Schilfgarde, A. Sher and A.-B. Chen, *J. Cryst. Growth*, 1997, **178**, 8.
- 17 L. K. Teles, J. Furthmüller, L. M. R. Scolfaro, J. R. Leite and F. Bechstedt, *Phys. Rev. B*, 2000, **62**, 2475.
- 18 J. A. Purton, G. D. Barrera, M. B. Taylor, N. L. Allan and J. D. Blundy, *J. Phys. Chem. B*, 1998, **102**, 5202.
- 19 M. Yu. Lavrentiev, N. L. Allan, G. D. Barrera and J. A. Purton, *J. Phys. Chem. B*, 2001, **105**, 3594.
- 20 D. Frenkel and B. Smit, *Understanding Molecular Simulation*, Academic Press, San Diego and London, 2nd edn., 2002.
- 21 N. I. Metropolis, A. W. Rosenbluth, M. N. Rosenbluth, A. Teller and E. Teller, *J. Chem. Phys.*, 1953, **21**, 1087.
- 22 P. Zapol, R. Pandey and J. D. Gale, *J. Phys. Condens. Matter*, 1997, **9**, 9517.
- 23 J. A. Chisholm, D. W. Lewis and P. D. Bristowe, *J. Phys. Condens. Matter*, 1999, **11**, L235.
- 24 P. Ruterana, B. Barbaray, A. Béré, P. Vermaut, A. Hairie, E. Paumier, G. Nouet, A. Salvador, A. Botchkarev and A. Morkoç, *Phys. Rev. B*, 1999, **59**, 15917.
- 25 J. Nord, K. Albe, P. Erhart and K. Nordlund, *J. Phys. Condens. Matter*, 2003, **15**, 5649.
- 26 F. H. Stillinger and T. A. Weber, *Phys. Rev. B*, 1985, **31**, 5262.
- 27 H. Xia, Q. Xia and A. L. Ruoff, *Phys. Rev. B*, 1993, **47**, 12925.
- 28 R. R. Reeber and K. Wang, *MRS Internet J. Nitride Semicond. Res.*, 2001, **6**, 3 (internet address nsr.mij.mrs.org). Reference has no page numbers.
- 29 *Properties of Group-III Nitrides EMIS data review series*, ed. J. H. Edgar, INSPEC, London, 1994, vol. 11.
- 30 K. Kim, W. R. L. Lambrecht and B. Segall, *Phys. Rev. B*, 1996, **53**, 16310.
- 31 F. M. Marquez, C. Cienfuegos, B. K. Ponsai, M. Yu. Lavrentiev, N. L. Allan, J. A. Purton and G. D. Barrera, *Modelling Simul. Mater. Sci. Eng.*, 2003, **11**, 115.